A fully passive nonlinear piezoelectric vibration absorber

Boris Lossouarn, Jean-François Deü, Gaëtan Kerschen

A fully passive nonlinear piezoelectric vibration absorber

B. Lossouarn[a,*], J.-F. Deü[a], G. Kerschen[b]

[a] *Laboratoire de Mécanique des Structures et des Systèmes Couplés, Conservatoire national des arts et métiers, Paris, France*
[b] *Department of Aerospace and Mechanical Engineering, University of Liège, Liège, Belgium*

Abstract

The objective this study is to develop the first fully passive nonlinear piezoelectric tuned vibration absorber (NPTVA). The NPTVA is designed to mitigate a specific resonance of a nonlinear host structure. To avoid the use of synthetic inductors which require external power, closed magnetic circuits in ferrite material realize the large inductance values required by vibration mitigation at low frequencies. The saturation of an additional passive inductor is then exploited to build the nonlinearity in the NPTVA. The performance of the proposed device is demonstrated both numerically and experimentally.

Keywords: Vibration damping, Nonlinear absorber, Piezoelectric shunt, Passive inductor

1. Introduction

Piezoelectric tuned vibration absorbers can effectively mitigate specific resonances [1–5] or multiple resonances [6–9] of linear mechanical systems. Yet, mechanical nonlinearities which can originate from, e.g., materials, large displacements and boundary conditions, are a frequent occurrence in engineering applications. These nonlinearities introduce mistuning that can significantly reduce vibration mitigation performance. Nonlinear vibration absorbers, among which we can cite the autoparametric vibration absorber [10, 11], the nonlinear energy sink [12–16] and other variants [17–23], represent an interesting alternative to linear vibration absorbers in view of their increased bandwidth.

In [24], Habib et al. developed the nonlinear tuned vibration absorber (NLTVA), which presents the unique feature that its nonlinearity possesses the same mathematical form as that of the primary system. Based on this absorber and its theoretical extension to piezoelectric absorbers [25], the present study aims at designing the first fully passive resonant shunt that synthesizes a cubic-like nonlinearity.

Instead of using a nonlinear capacitor, a physical inductor subjected to magnetic saturation is considered. An increase of the electrical current flowing through the shunt leads to a decrease of the equivalent inductance, which generates a hardening nonlinearity in the electrical domain. Through an adequate magnetic circuit, it becomes possible to approximate the principle of similarity [24] with purely passive electrical components.

The paper is organized as follows. The next section recalls the main features of the linear piezoelectric tuned vibration absorber and shows its limits for vibration mitigation of nonlinear structures. The concept of a nonlinear piezoelectric tuned vibration absorber (NPTVA) is introduced through a principle of nonlinear similarity with the host mechanical structure. While a NPTVA can be realized with a nonlinear capacitance, we show that a variable inductance can serve the same objective. Section 3 proposes to design a suitable fully passive nonlinear inductor using magnetic saturation. For demonstration, Section 4 considers an experimental beam possessing a cubic nonlinearity and covered with piezoelectric patches. A linear shunt with a single passive inductor is first built for vibration mitigation at low forcing amplitudes. For higher amplitudes, the designed saturable inductor is connected in series with a linear inductor to form the nonlinear piezoelectric shunt. Finally, conclusions are drawn in Section 5.

*Corresponding author
Email address: boris.lossouarn@lecnam.net (B. Lossouarn)

2. The nonlinear piezoelectric tuned vibration absorber (NPTVA)

2.1. The linear resonant shunt

A piezoelectric tuned vibration absorber consists of a piezoelectric element shunted with an inductor and a resistor in order to mitigate mechanical vibrations [1, 3, 4]. The shunt generates an electrical resonance that is tuned to the target mechanical resonance frequency. Considering a single-degree-of-freedom mechanical model, the resulting coupled system of equations can be written as follows,

$$\begin{aligned} m\ddot{u} + c\dot{u} + K^E u &= f + \frac{e^2}{C^\varepsilon}\left(\frac{q}{e} - u\right), \\ L\ddot{q} + R\dot{q} &= \frac{1}{C^\varepsilon}\left(eu - q\right), \end{aligned} \tag{1}$$

where u represents the mechanical displacement, q is the electric charge displacement and f is the excitation force. The constants m, c, K^E, L, R, C^ε and e are the mass, damping coefficient, stiffness in short circuit, inductance, resistance, piezoelectric capacitance and coupling coefficient, respectively. Those constants allow the calculation of a coupling factor

$$k_\mathrm{c} = \sqrt{\frac{\omega_\mathrm{O}^2 - \omega_\mathrm{S}^2}{\omega_\mathrm{S}^2}}, \quad \text{where} \quad \omega_\mathrm{S} = \sqrt{\frac{K^E}{m}} \quad \text{and} \quad \omega_\mathrm{O} = \sqrt{\frac{K^E + \frac{e^2}{C^\varepsilon}}{m}} \tag{2}$$

are the short-circuit and open-circuit natural frequencies, respectively. The natural frequency ω_O is actually deduced from Eq. (1) with $q = 0$, which corresponds to a zero-current condition. A minimization of the maximum displacement at constant forcing amplitude [3] then leads to an approximation for the optimal inductance and resistance values:

$$L = \frac{1}{C^\varepsilon \omega_\mathrm{O}^2} \quad \text{and} \quad R = \sqrt{\frac{3}{2}}\frac{k_\mathrm{c}}{C^\varepsilon \omega_\mathrm{O}}, \tag{3}$$

where we remark that the electrical resonance $1/\sqrt{LC^\varepsilon}$ has to be tuned to the open-circuit natural frequency ω_O. For vibration mitigation of a linear structure, the use of a linear resonant shunt tuned to its optimal inductance and resistance values offers an effective damping solution, as shown in Figure 1(a) which is computed from the numerical values in Table 1.

The resulting frequency response function, and thus the damping performance, does not depend on the excitation amplitude for a linear system. However, when a nonlinear stiffness is present, e.g., $K^E = K_0^E + K_\mathrm{NL}u^2$, the linear resonant shunt looses its effectiveness. Still based on the numerical values in Table 1, Figure 1(b) is obtained from time simulations involving a slow frequency-sweep excitation force. We observe a significant detuning of the linear absorber for increasing forcing amplitudes. Specifically, an increase in the amplitude of the second resonance peak occurs because of the varying mechanical resonance, while the electrical resonance frequency is kept constant. As shown in [24, 25], one can even observe at greater forcing amplitudes the merging of a detached resonance curve with the second peak, which leads to unacceptable vibration amplitudes. This paper develops a fully passive nonlinear piezoelectric tuned vibration absorber (NPTVA) to address the detuning of the linear device.

2.2. Principle of similarity through nonlinear capacitance

As shown theoretically and numerically for mechanical absorbers by Habib et al. [24, 26], the introduction of a nonlinear component into the tuned vibration absorber counteracts the effect of the nonlinearity of the primary system. According to the so-called "principle of similarity", the absorber should be governed by equations similar to those of the primary system. It means that the added nonlinearity should possess the same mathematical form as that of the original nonlinear system. For instance, if the nonlinearity in the host system is cubic or quintic, the absorber should possess a cubic or a quintic spring, respectively. Reference

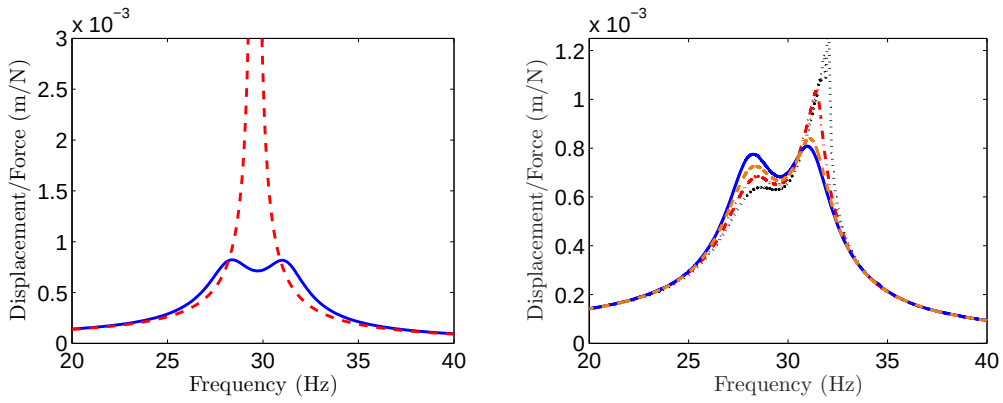

Figure 1: Frequency response functions with a linear piezoelectric tuned vibration absorber – (a) linear structure in short-circuit configuration (– –) and linear structure with an optimal linear shunt (—), (b) nonlinear structure with the linear shunt for various forcing amplitudes, $F = 0.2$ N (—), $F = 0.4$ N (– –), $F = 0.6$ N (– · –) and $F = 0.8$ N ($\cdots$).

[24] also provides a tuning rule that depends on ε, the mass ratio between the absorber and the primary structure:

$$\frac{k_{2i}}{k_{1i}} = \frac{(2\varepsilon)^{\frac{i-1}{2}}\varepsilon}{1 + 3.5 \times 1.5^{\frac{i-3}{2}}\varepsilon} \quad \text{for} \quad i \geq 2, \tag{4}$$

where k_{1i} and k_{2i} are the nonlinear spring coefficients of the primary system and of the absorber, respectively. Considering a cubic nonlinearity, i.e. $i = 3$, and a mass ratio $\varepsilon \ll 1$, we obtain $k_{23}/k_{13} \simeq 2\varepsilon^2$.

Based on this principle of similarity, a NPTVA possessing a nonlinear capacitance was proposed in [25]. For a primary system with cubic nonlinearity, we thus require a NPTVA with an electrical component providing a voltage proportional to q^3:

$$\begin{aligned} m\ddot{u} + c\dot{u} + K_0^E u + K_{\text{NL}} u^3 &= f + \frac{e^2}{C^\varepsilon}\left(\frac{q}{e} - u\right), \\ L_0\ddot{q} + R\dot{q} + \frac{1}{C_{\text{NL}}} q^3 &= \frac{1}{C^\varepsilon}\left(eu - q\right). \end{aligned} \tag{5}$$

where C_{NL} is the constant characterizing the nonlinear capacitor. While Eq. (4) does not strictly apply to a NPTVA, this tuning rule gives a suitable approximation for cases involving a nonlinear resonant shunt [25]. Here, the nonlinear spring coefficient of the primary system is $k_{13} = K_{\text{NL}}$ and the one of the nonlinear

Table 1: Numerical values for the mechanical, electrical and coupling parameters

Mechanical parameters		Electrical parameters	
m	0.3872 kg	L_0	106 H
c	0.3237 N.s/m	R	3050 Ω
K_0^E	13380 N/m	C^ε	268 nF
K_{NL}	2.507×10^9 N/m^3	C_{NL}	2.65×10^{-15} C^3/V
$\omega_{\text{S}}/2\pi$	29.59 Hz	α	8.65×10^3 A^{-2}
$\omega_{\text{O}}/2\pi$	29.82 Hz	β	6.50×10^{-4} V^{-1}
Coupling parameters			
e	7.55×10^{-3} C/m		
k_c	12.5 %		

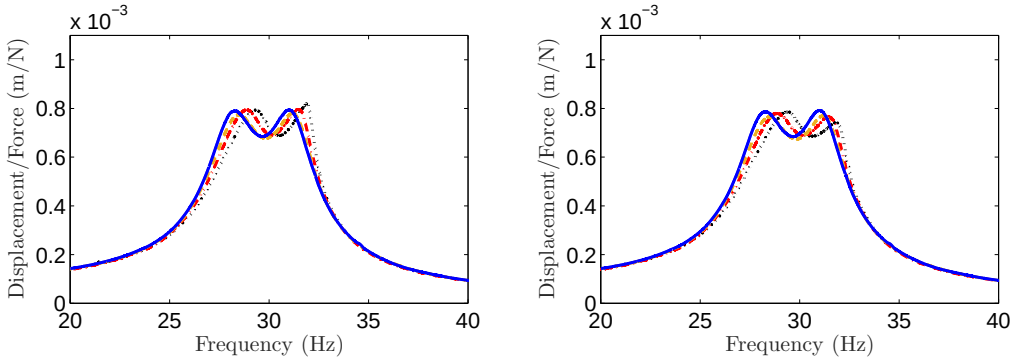

Figure 2: Simulated frequency response functions for various forcing amplitudes, $F = 0.2$ N (—), $F = 0.4$ N (– –), $F = 0.6$ N (– · –) and $F = 0.8$ N ($\cdots$) – (a) NPTVA with a nonlinear capacitor, (b) NPTVA with a nonlinear inductor.

absorber is $k_{23} = e^4/C_{\mathrm{NL}}$ in order to ensure dimensional homogeneity. For the same reason, the mass ratio is $\varepsilon = e^2 L_0/m$, which gives

$$\frac{1}{C_{\mathrm{NL}}} \simeq 2\left(\frac{L_0}{m}\right)^2 K_{\mathrm{NL}}, \tag{6}$$

when $e^2 L_0/m \ll 1$. Considering a NPTVA that satisfies Eq. (6), Figure 2(a) depicts a behavior close to the fully linear case, i.e., equal peaks can be maintained, which demonstrates the effectiveness of the NPTVA. Similar results can be obtained for other types of nonlinearity as long as the principle of similarity is considered [24, 25].

For a single resonance, a one-term harmonic balance approximation is usually enough [25]. We thus assume

$$q^\star = Q\sin(\omega t + \delta_q) \quad \text{and} \quad \left[\sin^3(\omega t + \delta_q)\right]^\star = \frac{3}{4}\sin(\omega t + \delta_q), \tag{7}$$

where the symbol $\star$ refers to the one-term harmonic balance approximation, Q is the electric charge displacement amplitude, ω is the angular frequency and δ_q is the phase constant. From Eqs. (5) and (7), we define the nonlinear voltage

$$v_{\mathrm{NL}}^\star = \frac{1}{C_{\mathrm{NL}}}\left[q^3\right]^\star = \frac{3}{4C_{\mathrm{NL}}} Q^3 \sin(\omega t + \delta_q), \tag{8}$$

which refers to the nonlinear electrical component that needs to be incorporated into the resonant shunt in order to compensate the mechanical nonlinearity through a principle of similarity.

2.3. Principle of similarity through nonlinear inductance

Capacitors offering a nonlinear relation between voltage and current can be found, but they exhibit a non-negligible linear contribution [27], which makes the practical implementation of the nonlinear voltage in Eq. (8) difficult. Another solution could be to use a synthetic impedance, but it requires a power supply, which may be bulky and does not prevent from potential stability issues. The purely passive solution considered herein exploits an inductor whose equivalent inductance value decreases with an increase of the electrical current $\dot{q}$ as

$$L(\dot{q}) = L_0\left(1 - \alpha\dot{q}^2\right). \tag{9}$$

The coupled system in Eq. (1) becomes

$$\begin{aligned} m\ddot{u} + c\dot{u} + K_0^E u + K_{\mathrm{NL}} u^3 &= f + \frac{e^2}{C^\varepsilon}\left(\frac{q}{e} - u\right), \\ L_0\ddot{q} + R\dot{q} - L_0\alpha\dot{q}^2\ddot{q} &= \frac{1}{C^\varepsilon}\left(eu - q\right). \end{aligned} \tag{10}$$

Adopting the one-term harmonic balance approximation in Eq. (7), the first harmonic of the nonlinear voltage is

$$v_{\mathrm{NL}}^{\star} = -L_0\alpha\left[\dot{q}^2\ddot{q}\right]^{\star} = \frac{L_0\alpha\omega^4}{4}Q^3\sin(\omega t+\delta_q). \tag{11}$$

A cubic relation similar to Eq. (8) is obtained if we ensure that

$$\frac{L_0\alpha\omega^4}{4} = \frac{3}{4C_{\mathrm{NL}}} \quad \text{so} \quad \alpha = 6\frac{L_0K^{\mathrm{NL}}}{m^2\omega^4}. \tag{12}$$

It thus turns out that a NPTVA involving an inductor with quadratic decrease can effectively mitigate the vibrations of a hardening system with cubic mechanical nonlinearity. This is confirmed by the simulations in Figure 2(b), which show that equal peaks are maintained for forcing amplitudes that would lead to a strong detuning of the corresponding linear shunt.

The equivalent inductance L_{eq} around the first harmonics is defined as

$$L_{\mathrm{eq}}\ddot{q}^{\star} = L_0\ddot{q}^{\star} + v_{\mathrm{NL}}^{\star}. \tag{13}$$

Knowing that $\ddot{q}^{\star} = -Q\omega^2\sin(\omega t+\delta_q)$, Eq. (11) gives a law for the equivalent variable inductance

$$L_{\mathrm{eq}} = L_0\left(1-\frac{\alpha}{4}\dot{Q}^2\right), \tag{14}$$

where $\dot{Q} = \omega Q$. The objective is then to design an inductor that approximates this variable inductance law for the implementation of a NPTVA.

3. Design of a nonlinear inductor based on magnetic saturation

Considering a physical inductor, magnetic saturation generates a decrease in its equivalent inductance value. In order to benefit from this property and to design a variable inductor dedicated to a NPTVA, it is first required to clarify the link between magnetic flux and equivalent inductance value. Then, material data provided by magnetic core manufacturers gives access to an estimation of the inductance nonlinearity.

3.1. From magnetic properties to equivalent inductance

As shown in Eq. (14), a decrease in the inductance value with respect to the current amplitude is required. Magnetic saturation can actually offer such a nonlinear dependence because the inductance is directly related to the magnetic flux Φ. While $\Phi = L\dot{q}$ in a linear case, as a more general rule

$$\Phi(\dot{q},\dot{q}_{\max}) = L_0(\dot{q}_{\max})\dot{q} + L_2\dot{q}^3 + L_4\dot{q}^5 + ... \tag{15}$$

The constants L_i are used to build an odd Taylor series approximating the nonlinear behavior of a magnetic field subjected to saturation. Also note, in $L_0(\dot{q}_{\max})$, the dependence to $\dot{q}_{\max}$ which refers to the maximum amplitude of the current $\dot{q}$. This represents the fact that, even before saturation, we observe a variation of the inductance that does not directly depend on $\dot{q}$ but on its maximum value. In practice, inductors made of ferrite magnetic material generate an equivalent inductance which first increases before saturation occurs. At such a low current, the relation between Φ and $\dot{q}$ remains linear but the slope increases with the amplitude of the electrical current [28]. This effect is due to a physical phenomenon called "wall movements" at the scale of the magnetic domains [29]. For this reason, the initial inductance L_0 can be described by a second Taylor series which depends on the maximum current through

$$L_0(\dot{q}_{\max}) = L_{00} + L_{01}\dot{q}_{\max} + L_{02}\dot{q}_{\max}^2 + ... \ , \tag{16}$$

a monotonically increasing function from L_{00} to a maximum value $L_0(\dot{q}_{\max}\to\infty) = L_0^{\infty}$. If only the first harmonic of the current $\dot{q}^{\star} = \dot{Q}\cos(\omega t-\delta_q)$ is retained, we have $\dot{q}_{\max}^{\star} = \dot{Q}$ so

$$\Phi^{\star} = \left(\left[L_{00}\dot{Q} + L_{01}\dot{Q}^2 + L_{02}\dot{Q}^3 + ...\right] + L_2\frac{3}{4}\dot{Q}^3 + L_4\frac{5}{8}\dot{Q}^5 + ...\right)\cos(\omega t-\delta_q). \tag{17}$$

As the equivalent inductance is defined from $\Phi^\star = \int L_{\rm eq}\ddot{q}^\star {\rm d}t = L_{\rm eq}\dot{q}^\star$,

$$L_{\rm eq} = L_{00} + L_{01}\dot{Q} + \left[L_{02} + \frac{3}{4}L_2\right]\dot{Q}^2 + L_{03}\dot{Q}^3 + \left[L_{04} + \frac{5}{8}L_4\right]\dot{Q}^4 + ... \tag{18}$$

Consequently, the nonlinear behavior of an inductor can be predicted from the description of the magnetic field as in Eq. (15) and the variable inductance in Eq. (16).

3.2. Exploitation of material data

Magnetic hysteresis curves are usually provided by core manufacturers. For example, Figure 3(a) shows the B-H relation in a T38 ferrite material (EPCOS), where B^m is the magnetic flux density and H^m is the magnetic field strength in the magnetic material. When neglecting the hysteresis behavior related to damping effects, the relation between B^m and H^m can be described by a monotonically increasing odd function $B^m = f\left(H^m\right)$. This function is not linear, unlike the B-H relation in the air $B^a = \mu_0 H^a$, where μ_0 is the vacuum permeability. As stated previously, we want to reconstruct the total magnetic flux in an inductor with n turns and an equivalent cross-section is A_e, which is defined by

$$\Phi = nBA_e \quad \text{where} \quad B = B^m = B^a \tag{19}$$

because of the continuity of the magnetic field density. Moreover, Ampere's law gives

$$n\dot{q} = \oint H dl = H^m l_e + H^a s \tag{20}$$

for a core of equivalent magnetic length l_e including an air gap $s \ll l_e$. For any value of the magnetic field strength H^m, the magnetic flux Φ and the current $\dot{q}$ can thus be computed from material and geometrical data through

$$\Phi = nA_e f(H^m) \quad \text{and} \quad \dot{q} = \frac{1}{n}\left(H^m l_e + \frac{s}{\mu_0} f(H^m)\right). \tag{21}$$

B-H curves such as the one in Figure 3(a) present a distinct magnetic saturation, which means that $L_0(\dot{q}_{\max})$ is close to its maximum value L_0^∞. So, the magnetic flux computed from Eq. (21) does not depend on $\dot{q}_{\max}$ anymore and Eq. (15) gives

$$\Phi(\dot{q}) = L_0^\infty \dot{q} + L_2\dot{q}^3 + L_4\dot{q}^5 + ... \tag{22}$$

Those constants are thus obtained from a polynomial approximation of the magnetic flux as a function of the electrical current.

On the other hand, material data generally gives access to the amplitude permeability $\mu_a = B_{\max}/H_{\max}$. An example amplitude permeability curve is shown in Figure 3(b) for the T38 material. After replacing H^m by $H^m_{\max}$ in Eq. (21), the maximum magnetic flux is expressed as

$$\Phi_{\max} = nA_e\mu_a H^m_{\max} \quad \text{and} \quad \dot{q}_{\max} = \frac{1}{n}\left(l_e + s\frac{\mu_a}{\mu_0}\right)H^m_{\max} \tag{23}$$

while Eqs. (15) and (16) lead to

$$\Phi(\dot{q}_{\max}) = L_{00}\dot{q}_{\max} + L_{01}\dot{q}^2_{\max} + \left[L_{02} + L_2\right]\dot{q}^3_{\max} + L_{03}\dot{q}^4_{\max} + \left[L_{04} + L_4\right]\dot{q}^5_{\max} + ... \tag{24}$$

So, with $\Phi_{\max} = \Phi(\dot{q}_{\max})$, all the constants in Eq. (24) can be obtained from a polynomial approximation of the maximum magnetic flux computed with the amplitude permeability. In the end, the nonlinear coefficient in Eqs. (22) and (24) leads to the equivalent inductance value in Eq. (18). As stated previously, this inductance needs to approach the variable inductance law in Eq. (14) for the implementation of a NPTVA. Note that a saturable inductor can still be completed with a linear inductor in series in order to reach an adequate low level inductance L_0, as performed in the following experiments.

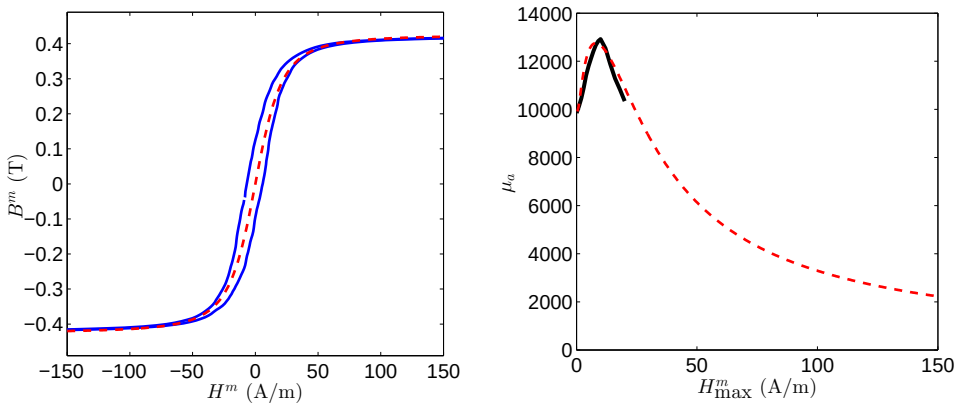

(a) (b)

Figure 3: Material data from EPCOS – (a) magnetic hysteresis loop (—) and its polynomial approximation (−−), (b) amplitude permeability (—) and its polynomial approximation (−−).

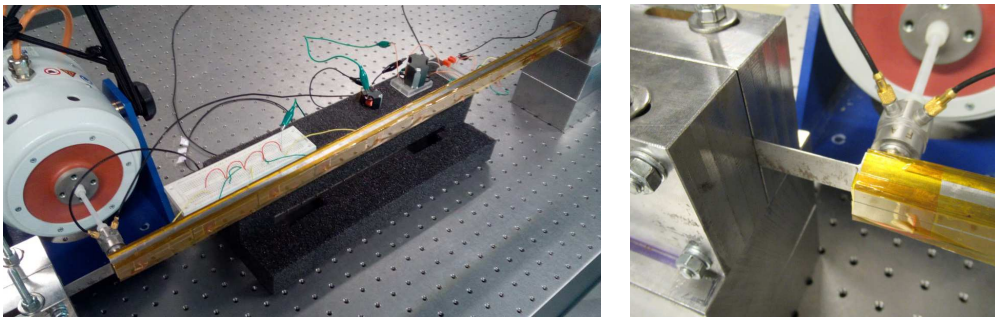

(a) (b)

Figure 4: Experimental setup – (a) cantilever beam with additional clamping through a thin lamina (left end), (b) focus on the thin lamina and the impedance head.

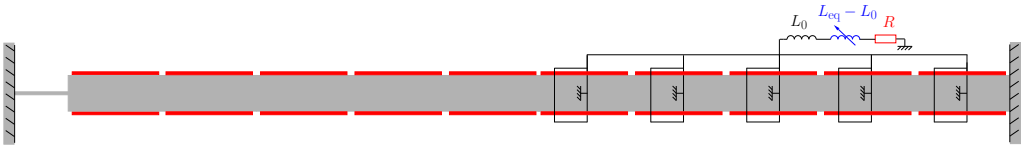

Figure 5: Half of the piezoelectric patches are connected in parallel and shunted with a linear inductor L_0, a resistor R and an additional nonlinear contribution $L_0 - L_{eq}$ when implementing a NPTVA.

4. Experimental setup based on a nonlinear piezoelectric beam

An experimental setup is proposed for validation of the NPTVA. The determination of the mechanical nonlinearity is first performed and the structure is coupled to a resonant piezoelectric shunt. While the linear shunt shows a strong detuning at high forcing amplitudes, the introduction of a properly designed saturable inductor increases the vibration mitigation performance.

4.1. Mechanical nonlinearity

The experimental setup in Figure 4(a) is made of a 700 mm long cantilever beam of cross-section area 14 mm × 14 mm [26, 30, 31]. This beam has been covered with an array of 2 mm thick PZT-5A bimorph

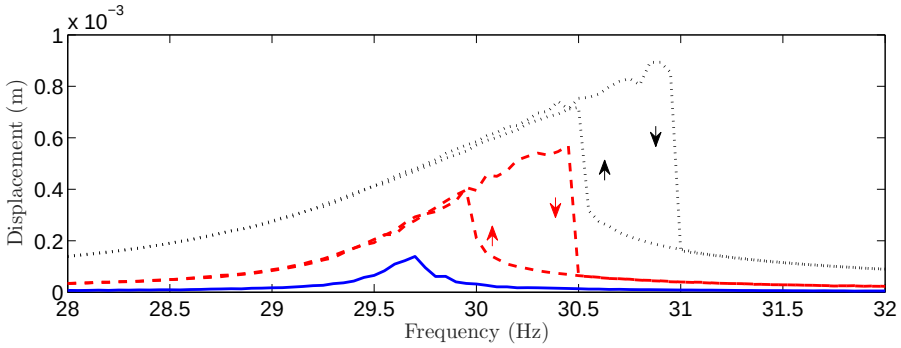

Figure 6: Displacement at the end of the nonlinear beam for various forcing amplitudes : $F = 0.01$ N (—), $F = 0.05$ N (−−), $F = 0.2$ N ($\cdots$).

patches for the implementation of a NPTVA. As represented in Figure 5, the twenty patches are placed all along the structure but only half of them are used in the following experiments in order to maximize piezoelectric coupling for the first mode of the cantilever beam. The mechanical nonlinearity is due to a thin lamina located at the free end of the beam, as shown in Figure 4(b). To determine the mechanical nonlinearity, the beam is excited with an electrodynamic shaker while an impedance head measures the input force and the resulting acceleration. Measurements are first performed with short-circuited piezoelectric patches in order to consider a purely mechanical problem around the first resonance of the beam. Indeed, Eq. (1) shows that a short circuit, i.e., $L = R = 0$, gives $q = eu$ and thus

$$m\ddot{u} + c\dot{u} + K_0^E u + f_{\text{NL}} = f, \tag{25}$$

where f_{NL} represents the nonlinear force contribution due to the thin lamina and K_0^E is the linear stiffness. The experimental results in Figure 6 are obtained from a stepped sine excitation with controlled forcing amplitude. They reveal a hardening nonlinearity that becomes significant when the displacement at the end of the beam exceeds 0.1 mm. Indeed, an hysteresis is observed through a jump phenomenon: the path followed by the displacement response is different for increasing or decreasing frequency of the sine excitation. Below 0.1 mm, however, the beam is almost linear and exhibits a resonance frequency around 29.6 Hz.

A low-level forcing frequency-sweep is then used to excite the beam around its first resonance with a sweep rate equal to 0.2 Hz/s. The acceleration signal is integrated in order to compute the velocity $\dot{u}$ and the displacement u. All the time signals are then filtered with a passband whose cutoff frequencies are 20 Hz and 40 Hz. The high-pass filtering aims at removing constant terms that appear through the numerical integration process and the low-pass filtering is used for being consistent with the theoretical part that focuses on a one-term harmonic balance approximation. This provides $\ddot{u}^\star$, $\dot{u}^\star$, $u^\star$ and $f^\star$ representing the first harmonic approximations of the primary time signals. Because the maximum displacement is around 0.1 mm, the nonlinear term in Eq. (1) is neglected and the constants are computed from the least-square solution of the system

$$\begin{bmatrix} m \\ c \\ K_0^E \end{bmatrix} = \left[\ddot{u}^\star \ \dot{u}^\star \ u^\star\right]^{-1} f^\star. \tag{26}$$

The modal parameters $m = 0.3872$ kg, $c = 0.3237$ N.s/m and $K_0^E = 13380$ N/m are found with a very low normalized mean-squared error [32] equal to 0.04 %. The mass and stiffness then lead to a natural frequency with short-circuited patches equal to $\sqrt{K_0^E/m}/2\pi = 29.59$ Hz.

The restoring force surface method is used to characterize the mechanical nonlinearity at higher excitation levels. Compared to the previous measurements, the forcing amplitude is multiplied by 10 so as to approach 1 mm for the maximum displacement at the end of the beam. The nonlinear restoring force $f_{\text{NL}}^\star$ is available

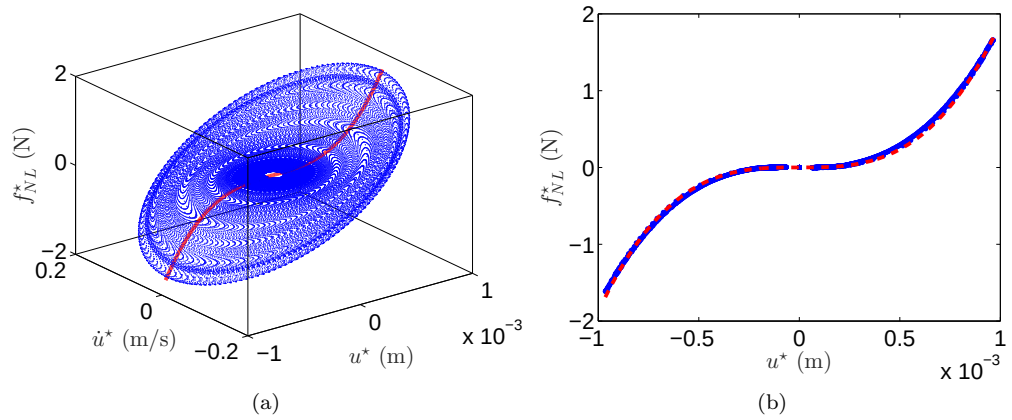

Figure 7: Experimental nonlinear restoring force (—) and cubic approximation (−−) – (a) three-dimensional representation as a function of u and $\dot{u}$, (b) restoring force when $\dot{u} = 0$.

as it can be computed from the filtered temporal series through

$$f^\star_{\mathrm{NL}} = f^\star - m\ddot{u}^\star - c\dot{u}^\star - K^E_0 u^\star \tag{27}$$

and its phase space representation is given in Figure 7(a). The two-dimensional section corresponding to $\dot{u}^\star = 0$ represented in Figure 7(b) highlights the cubic nonlinearity induced by the thin lamina: $f_{\mathrm{NL}} = K_{\mathrm{NL}} u^3$. Actually, a one-term harmonic balance approximation $u \simeq u^\star = U \sin(\omega t + \delta_u)$ means that

$$f^\star_{\mathrm{NL}} = K_{\mathrm{NL}} \left[u^{\star 3} \right]^\star . \tag{28}$$

A nonlinear coefficient $K_{\mathrm{NL}} = 2.507 \times 10^9$ N/m^3 is then obtained by filtering the signal $u^{\star 3}$ and solving Eq. (28) from a least-square method, which provides an excellent fit with a normalized mean-squared error equal to 0.4 %. Furthermore, from Eq. (7),

$$f^\star_{\mathrm{NL}}(\dot{u}^\star = 0) = \frac{3}{4} K_{\mathrm{NL}} u^{\star 3}, \tag{29}$$

which is the cubic approximation represented in Figures 7(a) and 7(b). This approximation offers a good correlation with the experimental measurements, which definitely validates the cubic form used to characterize the nonlinearity at the end of the beam.

4.2. Piezoelectric damping with a linear resonant shunt

Before considering a nonlinear shunt, a first step is to design a passive inductor that realizes a linear tuned vibration absorber when connected to the piezoelectric patches. To this end, it is required to determine the natural frequency of the beam when the piezoelectric patches are open-circuited. Low-level measurements similar to those with short-circuited patches lead to an open-circuit angular frequency $\omega_{\mathrm{O}} = \sqrt{K^D/m}$ where $K^D = K^E + e^2/C^\varepsilon$ as shown in Eq. (2). From the total piezoelectric capacitance which is around $C^\varepsilon = 268$ nF, the piezoelectric constant e can be calculated. Then, from the short-circuit and open-circuit resonance frequencies, $\omega_{\mathrm{S}}/2\pi = 29.59$ Hz and $\omega_{\mathrm{O}}/2\pi = 29.82$ Hz, respectively, the coupling ratio in Eq. (2) is $k_{\mathrm{c}} = 0.125$. Finally, from Eq. (3), the optimal shunt inductance and resistance are $L_0 = 106$ H and $R = 3050\ \Omega$. All the numerical values related to the primary mechanical structure, the electrical circuit and the coupling terms are summarized in Table 1.

A passive inductor with a magnetic circuit in ferrite material can satisfy the previous requirements [5]. For the present application, a RM14 magnetic core in N87 ferrite material (EPCOS) is selected. As it offers a permeance $A_L = L_0/n^2 = 1000$ nH, $n = 10^5$ turns of copper wire give access to an inductance value equal

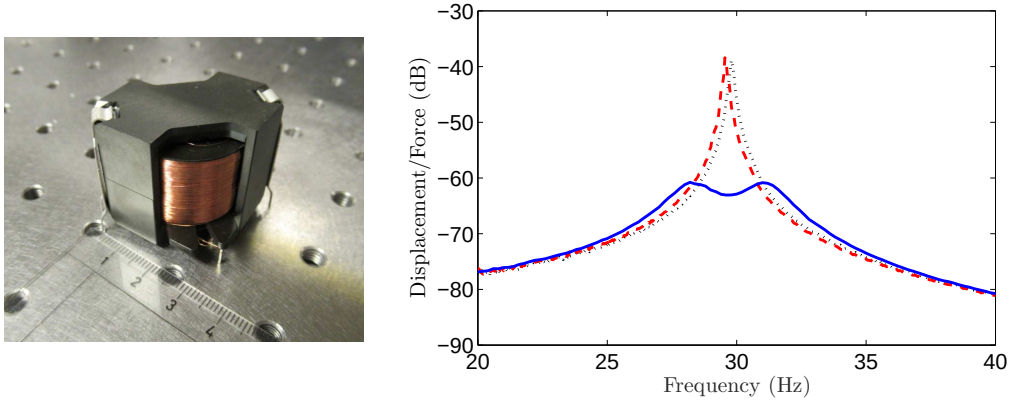

(a) (b)

Figure 8: Passive piezoelectric tuned vibration absorber – (a) physical inductor with a magnetic core in ferrite material, (b) experimental frequency response function around the first mechanical resonance, with short circuit (· · ·), with open circuit (· · ·) or with an optimal linear shunt for $F = 0.03$ N (—).

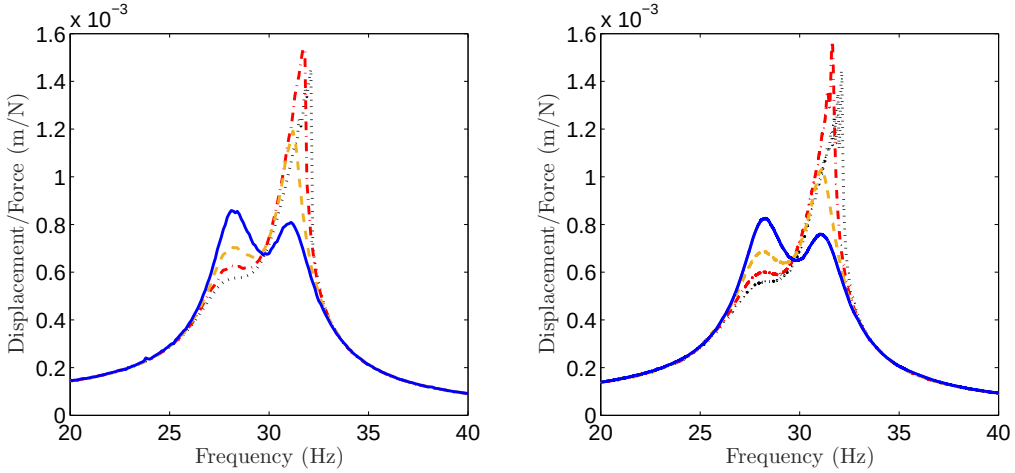

(a) (b)

Figure 9: Frequency response functions for various forcing amplitudes with a linear resonant shunt, $F = 0.2$ N (—), $F = 0.4$ N (– –), $F = 0.6$ N (– · –) and $F = 0.8$ N (· · ·) – (a) experiments, (b) simulations.

to 100 H at low excitation level. This is slightly below the required 108 H but the final tuning at low forcing amplitude is performed by adding a 20 nF capacitor in parallel with the piezoelectric patches in order to approach the angular frequency ω_O for the electrical resonance. A coil is thus made with 3 wires of 0.5 mm diameter in parallel, each of them representing 10^5 turns. The corresponding direct current resistance due to Joule effect in the copper wire is equal to 2100 Ω, which is below the optimal 3050 Ω. However, no external resistor was added to the shunt in order to prevent from any overdamped configuration that could result from additional damping in the magnetic material or in the piezoelectric patches. The inductor in Figure 8(a) is finally obtained and connected to the piezoelectric patches. Figure 8(b) shows a 23 dB vibration reduction compared to the cases with short- or open-circuited patches. Those results shows the efficiency of the piezoelectric tuned vibration absorber when the electrical resonance is correctly tuned to the mechanical one.

However, the results in Figure 9(a) show the limits of the linear shunt, which was tuned in order to

approximate an equal-peak configuration at low forcing amplitude. In accordance with Figure 1(b), increasing forcing amplitudes generate a strong detuning of the absorber. Actually, the detuning is even more significant in the present case because of a slight increase of both the piezoelectric capacitance and the inductance value. For the inductance, recall that our passive component is made of magnetic material that does not behave purely linearly, as shown in Eq. (16). Concerning the piezoelectric capacitance, it was experimentally noticed that it is also not constant when reaching high voltage amplitudes. Over the voltage range $0 \leq V \leq 100$ V, the capacitance variation can be approximated by

$$C^{\varepsilon} = C_0^{\varepsilon}(1 + \beta V), \tag{30}$$

where β is evaluated at 6.5×10^{-4} V^{-1}. While this variation is negligible below 10 V, the following experiments with a functional nonlinear shunt generate voltages up to 100 V. Equation (30) thus needs to be considered when designing the variable inductor for the implementation of a NPTVA. Furthermore, both the capacitance and inductance variations can be introduced into the electromechanical model developed in Section 2. This leads to the numerical results in Figure 9(b) that offer a good correlation with the experiments.

4.3. Variable inductance from material and experimental data

As the slight capacitance variation influences the electrical resonance, it needs to be introduced in Eq. (14) that represents the variable inductor law. Because we want to maintain $L_0 = 1/(C^{\varepsilon}\omega_0^2)$, from $\beta V \ll 1$, the corresponding Taylor series truncated to the first non-constant term is

$$L_{\text{eq}} = L_0 \left(1 - \beta L_0 \omega \dot{Q} - \frac{\alpha}{4}\dot{Q}^2\right), \tag{31}$$

where the voltage V has been replaced by $L_0\omega\dot{Q}$ after neglecting the resistance and nonlinear inductance contributions. All the numerical values are recalled in Table 1, where the constant α has been computed from Eq. (12). Represented in Figure 10(a), Eq. (31) gives the corrected variable inductance law for the design of a nonlinear inductor intended for the implementation of a NPTVA on the considered piezoelectric beam.

For the present application, two inductors are used to build the nonlinear shunt. A suitable saturable inductor is first selected and completed with an additional quasi-linear inductor. The considered magnetic core for the saturable inductor is a RM10 type in T38 material ($A_L = 1.6 \times 10^4$ nH). The coil is made of 1100 turns of wire with a 0.15 mm diameter. For the linear part, the same core as in the previous section is used but the number of turns is reduced to $n = 9130$. Following the method presented in Section 3, the expected equivalent inductance value of both inductors in series can be computed, which is represented in Figure 10(a). Even if the current dependence does not offer a quadratic decrease, inductors with magnetic saturation can definitely approximate the variable inductance law in Eq. (31) over a specific range of excitation.

The actual nonlinearity of the inductors is measured experimentally by applying an excitation voltage v and measuring the current $\dot{q}$ flowing through the components. The considered excitation is an harmonic voltage with varying amplitude from 0 to 100 V at a constant frequency equal to 30 Hz. After passband filtering between 20 Hz and 40 Hz, the equivalent inductance and resistance values are defined from

$$v^{\star} = L_{\text{eq}}\ddot{q}^{\star} + R_{\text{eq}}\dot{q}^{\star}, \tag{32}$$

where the filtered time signals are

$$v^{\star} = V\cos(\omega t + \delta_v), \quad \dot{q}^{\star} = \dot{Q}\cos(\omega t + \delta_{\dot{q}}) \quad \text{and} \quad \ddot{q}^{\star} = -\ddot{Q}\sin(\omega t + \delta_{\dot{q}}). \tag{33}$$

Consequently, the equivalent resistance and inductance values are

$$L_{\text{eq}} = \frac{V}{\ddot{Q}}\sin(\delta_v - \delta_{\dot{q}}) \quad \text{and} \quad R_{\text{eq}} = \frac{V}{\dot{Q}}\cos(\delta_v - \delta_{\dot{q}}). \tag{34}$$

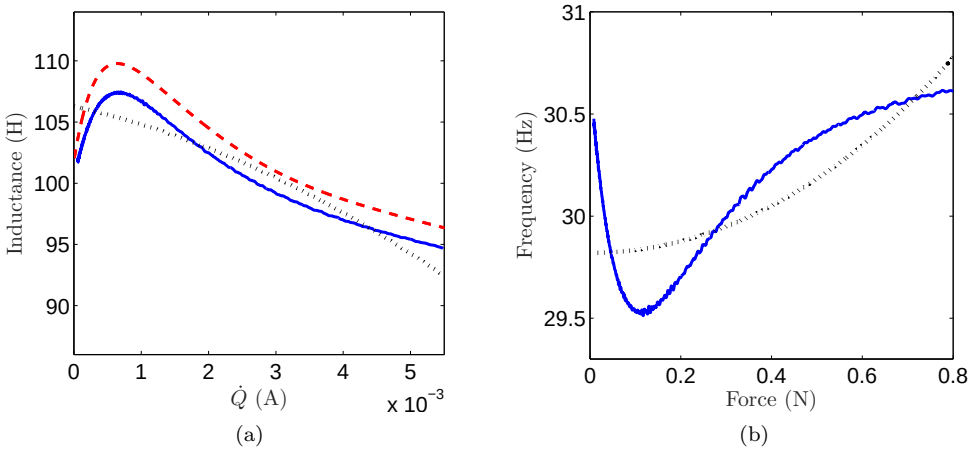

Figure 10: Equivalent inductance values and corresponding electrical resonance frequency – (a) inductance value from material data (−−), from experimental data (—) and variable inductance law (· · ·), (b) objective (· · ·) and experimental resonance frequency (—).

Those are computed by extracting the amplitudes V, $\dot{Q}$ and $\ddot{Q}$ as well as the phase shifts δ_v and $\delta_{\dot{q}}$. The result is a dependence of the equivalent values on the electrical current. The equivalent resistance R_{eq} varies from 2000 to 2500 Ω while the equivalent inductance is given in Figure 10(a) that validates the theoretical prediction from material data. As mentioned previously, even if the inductance does not offer a pure quadratic nonlinearity, the experimental results reveal that they are a sufficiently good approximation over the considered range of excitation.

The equivalent inductance value of the inductors gives access to the angular frequency of the resonant shunt ω_{exp} that is also influenced by the varying piezoelectric capacitance C^{ε}. Besides, the theoretical electrical angular frequency ω_{th} is defined from the variable inductance law in Eq. (14) which involves a pure quadratic decrease of the inductance value. Consequently,

$$\omega_{\text{th}}^2 = \frac{1}{L_0 C_0^{\varepsilon}\left(1 - \frac{\alpha}{4}\dot{Q}^2\right)} \quad \text{and} \quad \omega_{\text{exp}}^2 = \frac{1}{L_{\text{eq}} C_0^{\varepsilon}(1 + \beta Z_{\text{eq}}\dot{Q})}, \tag{35}$$

where $Z_{\text{eq}} = \sqrt{R_{\text{eq}}^2 + (\omega L_{\text{eq}})^2}$ is calculated at ω_{O}. From Eq. (1) at ω_{O}, $\dot{Q} = \frac{\omega_{\text{O}} C_0^{\varepsilon}}{e} F$, so that both theoretical and experimental frequencies can be plotted as functions of the input force. This is given in Figure 10(b), where crossings between the two curves predict optimal tuning of the electrical resonance, i.e. an equal peak condition on the mechanical response.

4.4. Performance of the nonlinear shunt

In the presence of the saturable inductor in the piezoelectric shunt, Figure 11(a) depicts that the NPTVA is able to maintain equal peaks over the considered range of forcing amplitudes. This is due to the decrease in the equivalent inductance value for increasing forcing amplitudes, hence the electrical resonance frequency is able to follow the increase in the mechanical resonance frequency as indicated in Figure 10(b). This is confirmed by the local minima of the frequency response functions which are moved toward higher frequencies. Furthermore, we note that depending on the forcing amplitude, the global maximum is either the left or the right peak. This phenomenon is explained by Figure 10(b), which shows the comparison between the actual electrical resonance and the theoretical objective that refers to the variable mechanical resonance. As mentioned previously, equal peaks are only expected when the two curves cross each other. This happens a first time between 0.2 N and 0.4 N, and a second time between 0.6 N and 0.8 N, which is verified in Figure 11(a), where we see transitions from a right maximum to a left maximum and conversely. Apart from

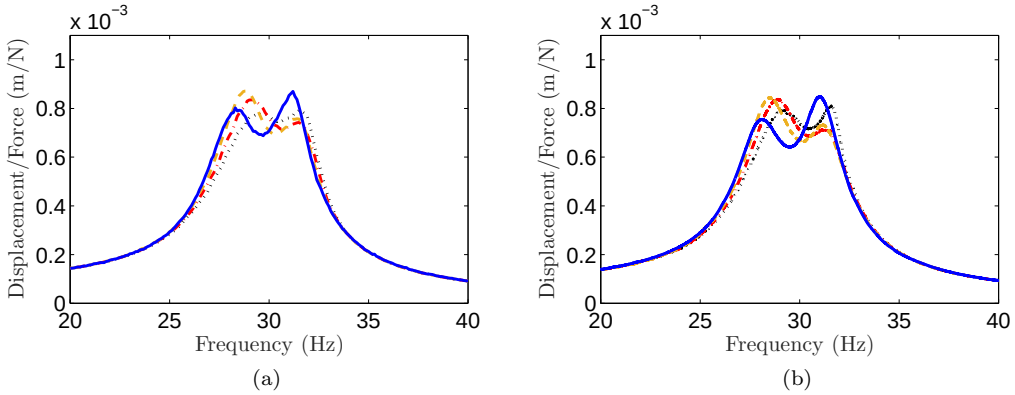

Figure 11: Frequency response functions for various forcing amplitudes with NPTVA based on a saturable inductor, $F = 0.2$ N (—), $F = 0.4$ N (– –), $F = 0.6$ N (– · –) and $F = 0.8$ N (· · ·) – (a) experiments, (b) simulations.

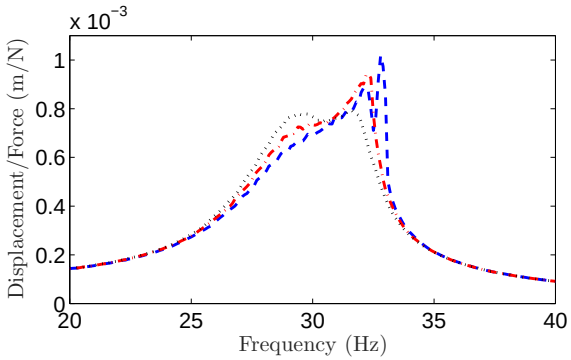

Figure 12: Experimental frequency response functions at higher levels causing adverse dynamics, $F = 0.8$ N (· · ·), $F = 1$ N (– · –) and $F = 1.2$ N (– –).

those slight variations, the amplitudes of the peaks in the frequency response functions do not present a clear dependence on forcing amplitude, as if the coupled system were obeying the superposition principle. Those experiments validate the concept of a NPTVA and more specifically its implementation with a saturable inductor. Moreover, the numerical results in Figure 11(b) show that integrating, into the electromechanical model, the inductance identified in Figure 10(a) provides a decent estimate of the frequency response functions at various amplitudes.

One still has to mention some limitations highlighted by the results in Figure 12. In the experiments, forcing excitations above 0.8 N lead to detuning of the NPTVA. A first reason is that the saturable inductor was designed for a specific range of excitation, i.e., from 0.1 N to 0.8 N. Beyond these values, the equivalent inductance deviates away from the variable inductor law in Eq. (31). This explains the increasing mistuning between the electrical and mechanical resonances that starts even before 0.8 N, as shown in Figure 10(b). A second reason is the occurrence of a merging between the second resonance peak and a detached resonance curve, which was illustrated in [24]. As a consequence, the NPTVA cannot maintain equal peaks over an infinite range of forcing amplitudes. Still, the NPTVA represents a substantial improvement over the linear absorber, as confirmed by the comparison between Figures 9 and 11.

5. Conclusions

The main objective of this study is to realize the first fully passive nonlinear piezoelectric tuned vibration absorber (NPTVA). Relying on the principle of nonlinear similarity, the NPTVA comprises a saturable

inductor whose equivalent inductance value depends on the electrical current flowing through the shunt. This results in a variable electrical resonance frequency that compensates the mechanical nonlinearity. Compared to a classical linear shunt, the nonlinear shunt is able to maintain an adequate tuning over a much wider range of forcing amplitudes. Eventually, the proposed NPTVA improves vibration mitigation without the need of power supply or external controller.

References

[1] Hagood NW, von Flotow A. 1991. Damping of structural vibrations with piezoelectric materials and passive electrical networks. *J. Sound Vib.* **146**.

[2] Hogsberg J, Krenk S. 2012. Balanced calibration of resonant shunt circuits for piezoelectric vibration control. *J. Intel. Mat. Syst. Str.* **23**.

[3] Thomas O, Ducarne J, Deü JF. 2012. Performance of piezoelectric shunts for vibration reduction. *Smart. Mater. Struct.* **21**.

[4] Soltani P, Kerschen G, Tondreau G, Deraemaeker A. 2014. Piezoelectric vibration damping using resonant shunt circuits: an exact solution. *Smart Mater. Struct.* **23**.

[5] Lossouarn B, Aucejo M, Deü, JF, Multon B. 2017. Design of inductors with high inductance values for resonant piezoelectric damping. *Sensor. Actuat. A-Phys.* **259**.

[6] Wu SY. 1998. Method for multiple mode piezoelectric shunting with single PZT transducer for vibration control. *J. Intel. Mat. Syst. Str.* **9**.

[7] Porfiri M, dell'Isola F, Frattale Mascioli FM. 2004. Circuit analog of a beam and its application to multimodal vibration damping, using piezoelectric transducers. *Int. J. Circ. Theor. App.* **32**.

[8] Lossouarn B, Deü JF, Aucejo M. 2015. Multimodal vibration damping of a beam with a periodic array of piezoelectric patches connected to a passive electrical network. *Smart Mater. Struct.* **24**.

[9] Lossouarn B, Deü JF, Aucejo M, Cunefare KA. 2016. Multimodal vibration damping of a plate by piezoelectric coupling to its analogous electrical network. *Smart Mater. Struct.* **25**.

[10] Oueini S, Nayfeh A. 2000. Analysis and application of a nonlinear vibration absorber. *J. Vib. Control* **6**.

[11] Vyas A, Bajaj AK. 2001. Dynamics of autoparametric vibration absorbers using multiple pendulums. *J. Sound Vib.* **246**.

[12] Vakakis AF, Gendelman OV. 2001. Energy pumping in nonlinear mechanical oscillators, Part II: resonance capture. *J. Appl. Mech.* **68**.

[13] Vakakis AF, Gendelman O, Bergman LA, McFarland DM, Kerschen G, Lee YS. 2009. *Nonlinear targeted energy transfer in mechanical and structural systems*. Springer, Series: Solid Mechanics and Its Applications.

[14] Gourdon E, Alexander NA, Taylor C, Lamarque CH, Pernot S. 2007. Nonlinear energy pumping under transient forcing with strongly nonlinear coupling: theoretical and experimental results. *J. Sound Vib.* **300**.

[15] Bellet R, Cochelin B, Herzog P, Mattei PO. 2010. Experimental study of targeted energy transfer from an acoustic system to a nonlinear membrane absorber. *J. Sound Vib.* **329**.

[16] Gourc E, Seguy S, Michon G, Berlioz A. 2013. Chatter control in turning process with a nonlinear energy sink. *Adv. Mat. Res.* **698**.

[17] Shaw J, Shaw SW, Haddow AG. 1989. On the response of the non-linear vibration absorber. *Int. J. of Nonlin. Mech.* **24**.

[18] Ema S, Marui E. 1996. A fundamental study on impact dampers. *Int J. Mach. Tool. Manu.* **36**.

[19] Collette FS. 1998. A combined tuned absorber and pendulum impact damper under random excitation. *J. Sound Vib.* **216**.

[20] Poovarodom N, Kanchanosot S, Warnitchai P. 2003. Application of non-linear multiple tuned mass dampers to suppress man-induced vibrations of a pedestrian Bridge. *Earthq. Eng. Struct. D.* **32**.

[21] Alexander NA, Schilder F. 2009. Exploring the performance of a nonlinear tuned mass damper. *J. Sound Vib.* **319**.

[22] Lacarbonara W, Cetraro M. 2011. Flutter control of a lifting surface via visco-hysteretic vibration absorbers. *Int. J. Aeronaut. Space* **12**.

[23] Ducarne J, Thomas O, Deü JF. 2010. Structural vibration reduction by switch shunting of piezoelectric elements: modeling and optimization. *J. Intel. Mat. Syst. Str.* **21**.

[24] Habib G, Kerschen G. 2016. A principle of similarity for nonlinear vibration absorbers. *Physica D* **332**.

[25] Soltani P, Kerschen G. 2015. The nonlinear piezoelectric tuned vibration absorber. *Smart. Mater. Struct.* **24**.

[26] Habib G, Grappasonni C, Kerschen G. 2016. Passive linearization of nonlinear resonances. *J. Appl. Phys.* **120**.

[27] Gluskin E. 1985. The use of non-linear capacitors. *Int. J. Electron.* **58**.

[28] Legg VE. 1936. Magnetic measurements at low flux densities using the alternating current bridge. *Bell Labs Tech. J.* **15**.

[29] Ducharne B, Le MQ, Sebald G, Cottinet PJ, Guyomar D, Hebrard Y. 2017. Characterization and modeling of magnetic domain wall dynamics using reconstituted hysteresis loops from Barkhausen noise. *J Magn. Magn. Mater.* **432**.

[30] Thouverez F. 2003. Presentation of the ECL benchmark. *Mech. Syst. Signal Pr.* **17**.

[31] Grappasonni C, Habib G, Detroux T, Kerschen G. 2016. Experimental demonstration of a 3D-printed nonlinear tuned vibration absorber. In: *Nonlinear Dynamics* **1**, Conference Proceedings of the Society for Experimental Mechanics Series, Springer, Cham.

[32] Kerschen G, Lenaerts V, Golinval JC. 2003. VTT benchmark: application of the restoring force surface method. *Mech. Syst. Signal Pr.* **17**.